Nascent Phase Separation and Crystallization Kinetics of an iPP/PEOc Polymer Alloy Prepared on a Single Multicatalyst Reactor Granule

Jiang Du,[†] Hui Niu,[‡] Jin-Yong Dong,*[,‡] Xia Dong,[†] Dujin Wang,[‡] Aihua He,[†] and Charles C. Han*[,†]

State Key Laboratory of Polymer Physics and Chemistry, Joint Laboratory of Polymer Science and Materials, Institute of Chemistry, Chinese Academy of Sciences, Beijing 100080, China, and CAS Key Laboratory of Engineering Plastics, Joint Laboratory of Polymer Science and Materials, Institute of Chemistry, Chinese Academy of Sciences, Beijing 100080, China

Received September 30, 2007; Revised Manuscript Received December 17, 2007

ABSTRACT: The crystalline morphology and the liquid−liquid phase separation (LLPS) of an isotactic polypropylene/poly(ethylene-*co*-octene) (iPP/PEOc) polymer alloy prepared on a single multicatalyst reactor granule were studied by polarized optical microscope, phase contrast optical microscope, and scanning electron microscopy (SEM). We found that the LLPS process had a dominant effect on the final crystalline morphology of the iPP/PEOc polymer alloy. As the LLPS time was increased at 160 °C, more and more elastomer component was dispersed uniformly in the iPP spherulites as droplets, instead of being rejected to the outside and concentrated at the boundaries of the spherulites, when the sample was isothermally crystallized at 140 °C. The morphologies can be explained by the phase separation and crystallization kinetics. By simply changing the LLPS time, we could control the size of the elastomer droplets (for example between 1 and 10 μm) that dispersed in the iPP spherulites. Meanwhile, a special structural feature which had different iPP spherulites linked together by numerous iPP fibers separated by interconnected elastomer domains was observed by SEM. This in-reactor blending/alloying process provides a new initial state (nascent state) which is not obtainable by conventional solution blending or extruder blending processes for the study of phase separation and crystallization processes in a polyolefin alloy and also provides a flexible and maybe better way to control the structure, dispersion, and finally the properties of elastomer toughened iPP alloys in application.

Introduction

Polypropylene (PP) is an important commercial plastic and is widely used for its low price and good properties (processability, chemical resistance, low density, etc.). However, its intrinsic flaws, especially its poor low-temperature impact strength, have significantly hindered its usage. Various approaches have been tried to improve its toughness and durability. One extensively used method is to modify PP by copolymerizing propylene with low content of other α-olefins to produce high-impact polypropylene copolymers or block copolymers.[1−3] Other methods include creating a heterophasic polymer system containing different, preformed polyolefins compatible with the polypropylene by mechanical blending.[4−15] However, the compounding technique is normally energy intensive and expensive; also, the improvement is often limited.

In the 1990s, Montell Co. developed an in-reactor blending technique named Catalloy process.[16−18] Polyolefin alloys were made from the monomers directly in the reactor, replacing the polymer blends previously made by melt mixing from component polymers. A spherical, superactive $TiCl_4/MgCl_2$-based catalyst was used, and multiphase, multipolymer PP alloys with spherical shape were produced in a multistage polymerization process. In the first stage, iPP particles were produced, and in the second stage, a rubbery copolymer phase was produced within the preformed iPP matrix. Later, Montell Co. successfully alloyed polyolefins with non-olefinic materials in the reactor by Hivalloy process.[17] The products combined the most desirable properties of polypropylene with many desirable characteristics of engineering resins. In 1997, a process named multicatalyst reactor granule technology (MRGT) was reported,[19] in which Ti-based catalysts and metallocene catalysts were both used. In these processes, the rubber phase was formed directly in the iPP spherical particles; supposedly, it could reach a high degree of dispersion in these alloys, resulting in a more intimate interaction between the matrix and the rubber phase. These processes allow a wider range of rubber content in the alloys and better control over the phase structure. Compared to PP blends formed by mechanical blending, blends prepared by in-situ or in-reactor blending techniques have been proved to be superior in both mechanical properties and production costs.[16−22]

Although the MRGT combines the advantages of different catalysts, the complex processes make it challenging to scale up industrial use. Moreover, the metallocene compound could not be dispersed well in the porous iPP particles through an impregnation process. An alternative multistage process (single multicatalyst reactor granule technology) which is capable of producing a wide range of olefin polymer compositions has been worked out in our laboratory, with a different catalytic system (Ti/Zr hybrid catalysts) in a two-stage process.[23] In particular, in the first stage, iPP was prepared selectively by the Ziegler−Natta component of the Ziegler−Natta/metallocene hybrid catalyst, while the metallocene component was blocked by an inhibitor. In the second stage, one or more olefins were polymerized in the presence of the product obtained from the first stage, after the reactivation of the metallocene component by a reactivator. This two-stage process has industrial potential.

Turning to the compositional heterogeneity, chain structure, and properties of the in-reactor prepared PP alloys, some studies have been already reported;[20,24−27] however, very few papers

* To whom all correspondence should be addressed. E-mail: c.c.han@iccas.ac.cn. E-mail: jydong@iccas.ac.cn.
[†] State Key Laboratory of Polymer Physics and Chemistry.
[‡] CAS Key Laboratory of Engineering Plastics.

10.1021/ma7021869 CCC: $40.75
Published on Web 02/02/2008

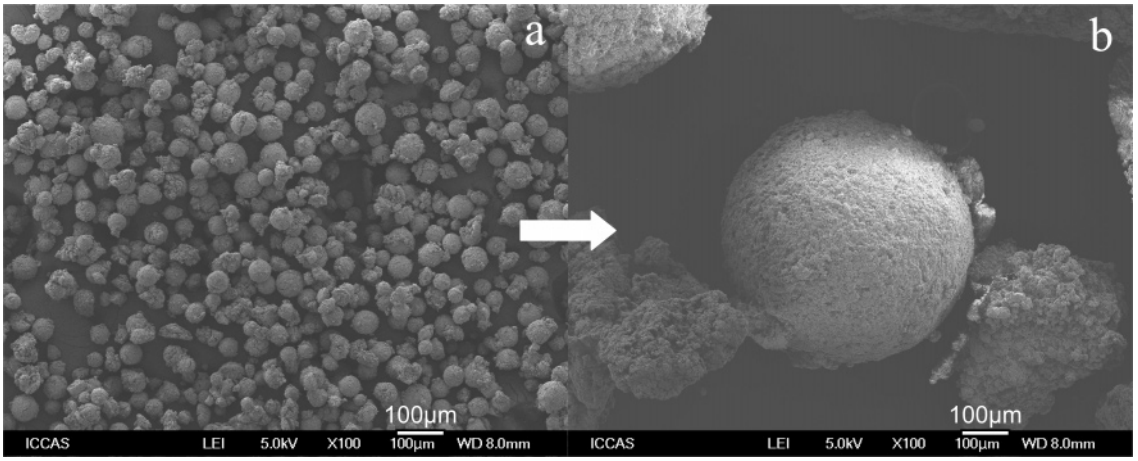

Figure 1. SEM images of the primary catalyst particles (a) and the product iPP/PEOc polymer blend spheres (b). The scale bar is 100 μm.

were actually focused on the morphology of this kind of polymer alloy.[21,28] As is well-known, the effectiveness of toughening plastic by blending with elastomer depends on the morphology of the blend, such as the shape, size, and distribution of the dispersed phase, the morphology of the crystalline matrix, and the degree and nature of adhesion between different phases.[29−32] High-impact PP, produced either by copolymerization of propylene with other α-olefins or by blending PP with various elastomers, normally has a biphasic or multiphasic structure. The morphology of the product has a great effect on its properties.[22,29,30,33−36] The in-reactor prepared PP alloy is a more complicated system. Its excellent properties rely on the special nascent micro- and nanoscale phase structure. It is necessary to study the phase separation, the crystalline morphology, their kinetics, and mechanism thoroughly in order to be able to control the final properties through the control of the structure/morphology. In this work, we studied the characteristic phase separation, crystalline morphology, and the LLPS effect on the crystallization of the hybrid catalyst prepared iPP/PEOc in-reactor polymer alloy by polarized optical microscope, phase contrast optical microscope, and SEM methods. The LLPS process provided systematic control over the final crystalline morphology. Some special phase structures were observed for the first time.

Experimental Section

Material and Sample Preparation. A two-stage polymerization was conducted using high activity $MgCl_2-TiCl_4/Et(Ind)_2ZrCl_2$ hybrid catalysts.[23] The iPP/PEOc polymer blend particles were directly obtained in reactor after the homopolymerization and the subsequent copolymerization processes. The weight-average molecular mass was 2.0×10^5, and the polydispersity index (weight-average molecular mass/number-average molecular mass) of the blend was 3.23, measured by GPC. The average elastomer content of the iPP/PEOc particles was 15 wt %. The blend particles were hot-pressed at 200 °C to form films of 20 μm in thickness (for optical microscopy) and then quenched to room temperature for further use.

Morphology Analysis. The polarized optical microscopy (POM) observations were carried out using Nikon (L-UEPI) optical microscope with Nikon (COOLPIX4500) camera. The phase contrast optical microscopy (PCOM) observations were carried out using Olympus (BX51) optical microscope and Olympus (C-5050ZOOM) camera. A Linkam (350) hot stage was used to control the sample temperature. In a typical optical observation, a sample was heated to 200 °C for 10 min to erase thermal history and then quenched to the selected LLPS temperature of 160 °C for annealing with different times. After annealing, the sample was isothermally crystallized at 140 °C.

For SEM observation, the sample was coated with Pt and then observed by a JEOL 6700F scanning electron microscope at an accelerating voltage of 5 kV. Some samples were etched by *n*-heptane for 72 h at room temperature before observation.

Results and Discussion

Figure 1 is the SEM images of the primary catalyst particles (Figure 1a) and the resulting iPP/PEOc heterophase polymer spheres (Figure 1b). It can be seen that both the catalyst particles and the polymer spheres are spherical in shape, indicating that the original spherical morphology of the catalyst is replicated in the final polymer product as the particle growth takes place during the polymerization. The dimensions of the primary catalyst particles range from 20 to 80 μm, while the diameters of the product polymer spheres range from 500 to 2000 μm. The spherical form is the most attractive one for many reasons. For example, it is the best form to increase the flowability of polymers during processing, and the spherical form polymers obtained are utilizable without any pelletization operation, which is expensive and could cause polymer overheating, impairing the quality of the final product.

The iPP/PEOc blend spheres were hot-pressed to films and heat-treated in a hot stage for crystalline morphology observation. Figure 2 shows the overview of the well-developed large size iPP spherulites grown from the melt following two different thermal treatments. In Figure 2a, the sample was first heated to 200 °C for 10 min to erase its thermal history, and then it was quenched directly to 140 °C for isothermal crystallization. In Figure 2b, after erasing thermal history at 200 °C, the sample was quenched to a selected LLPS temperature of 160 °C and annealed for 12 h. After annealing, it was quenched to 140 °C for isothermal crystallization. Well-developed iPP spherultes, which had the characteristics of a continuous sheaflike texture aligning radially outward, were clearly observed in both micrographs. However, the morphology of the spherulite boundaries was obviously different. In Figure 2a, there were clear separation bands between neighboring spherulites, which could not get into an intimate touch with each other. In Figure 2b, the area of the interspherulitic region diminished sharply. The boundaries became blurred and presented an intermittently connected structure. Neighboring iPP spherulites contacted with each other much more closely than those in Figure 2a. These interspherulitic regions, both in Figure 2a and Figure 2b, should be the noncrystallizable elastomer-rich areas. It is known that the basis for the phenomenon of spherulitic crystallization is the tendency for the polymer to reject noncrystallizable material from the crystallization front during their formation.[37] As a

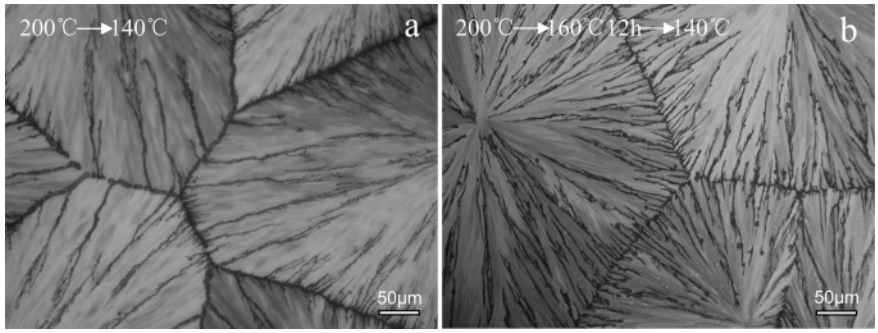

Figure 2. Polarized optical micrographs showing the overview of the spherulites and the different morphology of the spherulite boundaries of samples with different thermal treatments.

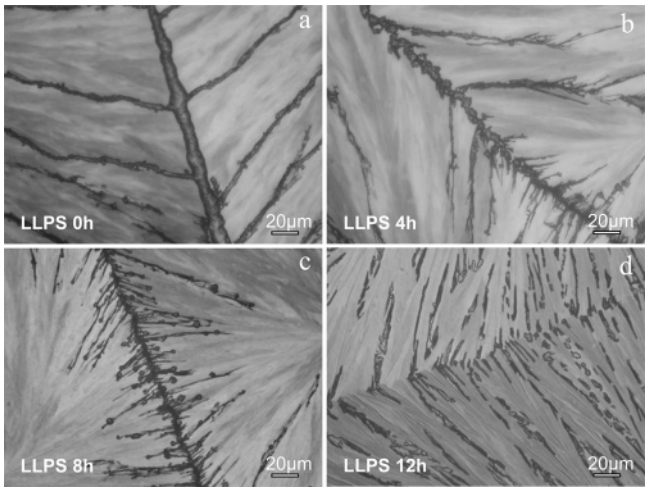

Figure 3. Polarized optical micrographs showing the detailed morphologic differences of the spherulite boundaries of samples with different thermal treatments.

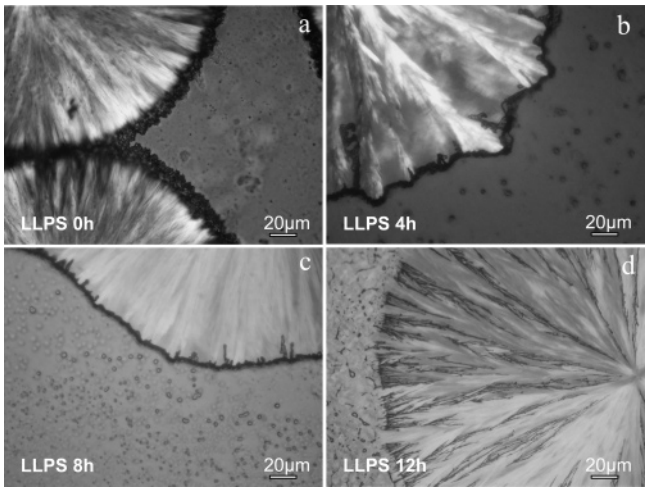

Figure 4. Polarized optical micrographs: the PEOc-rich layer at the growth front of the iPP spherulite.

result, the rejected noncrystallizable material becomes concentrated at the boundaries between adjacent spherulites. This was verified in the latter sections by etching technique and SEM observation (see Figure 10). So it seems that much more PEOc elastomer component would be rejected outside the iPP spherulites if the sample was directly quenched from 200 to 140 °C for isothermal crystallization. On the contrary, it seems that most PEOc component would deposit and disperse inside the iPP spherulites if the sample underwent LLPS at 160 °C for 12 h before isothermal crystallization at 140 °C. It indicates that after LLPS the PEOc elastomer component probably phase-separated and coarsened to droplet sizes too large to be pushed and rejected by the growth front of the iPP spherulites and consequently dispersed inside the spherulites during the isothermal crystallization process.

Under higher magnification, Figure 3 shows the fine morphological differences of the boundaries between two adjacent iPP spherulites. The samples were isothermally crystallized at 140 °C after LLPS at 160 °C for 0 (a), 4 (b), 8 (c), and 12 h (d). From the polarized optical micrographs, it can be seen clearly that the spherulite boundaries gradually changed their shapes, from a wide coherent separation band to a blurred intermittent borderline, as the LLPS time was increased from 0 to 12 h step by step. As shown in Figure 3a, two adjacent spherulites were separated completely from each other by a pronounced interspherulitic region. This region between the edges of the spherulites was about 10−15 μm wide. As mentioned above, it was the noncrystallizable material-rich area containing a high concentration of the PEOc elastomer, which was rejected out by the growing crystals due to the fractionation or segregation effects. When the LLPS time was increased from 0 to 4 h, the width of the boundary reduced sharply to about 5−8 μm. The boundary was no longer a coherent band. It was made up of many small blocks of elastomer component and shaped like a knotty line, as shown in Figure 3b. When the LLPS time was increased to 8 h, the width of the boundary further reduced to about 3−5 μm. As shown in Figure 3c, the boundary also presented a kind of knotty line structure, but each single knot was much smaller than that in Figure 3b. When the LLPS time extended to 12 h, the boundary became blurred. The noncrystallizable elastomer-rich areas shrunk to some isolated domains along the interface. Neighboring spherulites became partially connected with each other directly, as shown in Figure 3d. On the other hand, it can be seen that there were several branch veins on either side of the spherulite boundary. These intraspherulite branch veins originated from the inner part of the spherulites and orientated toward the outside of the spherulites, paralleling to the growth direction of the lamella and "flowing" into the interspherulite boundary in the end. It confirms that the interspherulite boundaries are the confluence of the elastomer component rejected out through the growth of lamella. As the LLPS time was increased from 0 to 12 h, these branch vein regions also shrunk gradually like the boundaries. It implies that as the LLPS time was increased, less and less elastomer component was rejected out of the spherulites during the crystallization process, resulting in the shrink of the boundaries and the branch veins.

In order to further prove the deduction obtained above, the optical microscopic observation was focused on the growth front of the growing iPP spherulites (Figure 4). The samples were isothermally crystallized at 140 °C for the same time (10 h)

after LLPS at 160 °C for 0 (a), 4 (b), 8 (c), and 12 h (d). It can be seen that there was a distinct noncrystallizable material-rich layer at the growth front of the iPP spherulite when the sample was directly crystallized without the LLPS process, as shown in Figure 4a. This gives direct evidence that the elastomer PEOc component was rejected outside the iPP spherulite during crystallization. After LLPS for 4 h, when the sample was crystallized for the same time, the PEOc-rich layer at the growth front of the spherulite diminished visibly, as shown in Figure 4b. This indicates that less amount of the PEOc component was pushed out of the spherulite. As the LLPS time was increased to 8 h, the PEOc-rich layer at the growth front of the spherulite, compared to Figure 4a and Figure 4b, diminished further after the same crystallization time, as shown in Figure 4c. And when the LLPS time extended to 12 h, the PEOc-rich layer at the growth front of the spherulite almost disappeared, as shown in Figure 4d. These results directly show that less and less elastomer component accumulated at the growth front of the spherulite during crystallization as the prior LLPS time was increased from 0 to 12 h. It confirms that the elastomer component was more and more difficult to be rejected with the LLPS time.

The discussions above indicate that the LLPS process has a great effect on the subsequent crystallization. The following measurements were carried out to clarify the LLPS process of this system and its relationship with the crystallization. Samples were heated to 200 °C to erase thermal history first. Then they were annealed at 160 °C for LLPS for different times. The samples were taken out from the hot stage after different annealing time and quenched to room temperature to freeze in the phase structure for the subsequent observation by a phase contrast microscope. The morphological development was found as follows (shown in Figure 5). Many small droplets, smaller than 1 μm in diameter, appeared from an initially homogeneous mixture soon after the sample was quenched to the LLPS temperature. It is noticeable that the distribution of droplet size was narrow at first. With the lapse of time, droplets kept on growing in size, meanwhile broadening in the size distribution. It can be observed that different sizes of droplets coexisted especially in samples e and f.

We believe the above phenomena are consistent with an off-critical LLPS (85/15 of iPP/PEOc) in the unstable region. The characteristic length scale, $l(t)$, for the phase-separation process can be obtained from the images via a fast Fourier transform (FFT) analysis. The 2D FFT images are shown as insets in Figure 5. Radially averaged profiles give the predominant wave vector, q_m, with $l = 2\pi/q_m$, which grows with time, as shown in Figure 6. For monodispersed spheres randomly distributed in a homogeneous medium, the $2\pi/q_m$ should be a close approximation for the first peak (exact $(qR)_{max} = 5.76$). This dimension corresponds to the radius of the sphere instead of the separation distance. The interesting result here is the nonlinear time growth of the domain size; i.e., the increase rate of l becomes smaller with time t. At beginning, it grows linearly with time, $l \propto t$. At late times, the growth curve approaches the straight line with the slope near $^1/_3$, indicating the growth law crosses over to a collision−coalescence form. It is a slower diffusive growth process and also causes the broadening of the droplets size distribution.

We should point out that the size of the elastomer rich droplets and the small optical contrast between PP and PEOc limit the analysis at relatively early times, where the elastomer phase should be cocontinuous. We only vaguely observed the hydrodynamic flow dominated breakup region ($\sim t^1$), and the late stage

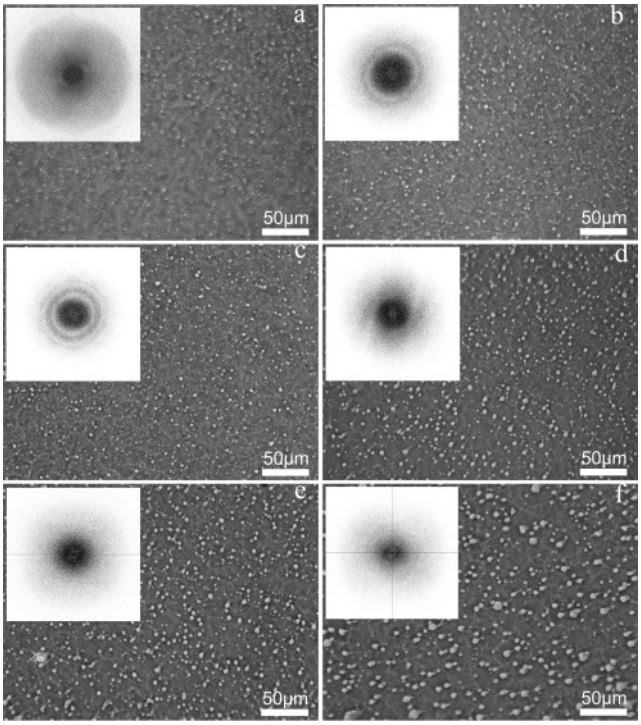

Figure 5. Phase contrast optical micrographs of the iPP/PEOc in-reactor polymer blend after annealing at 160 °C for (a) 2, (b) 4, (c) 8, (d) 12, (e) 24, and (f) 48 h.

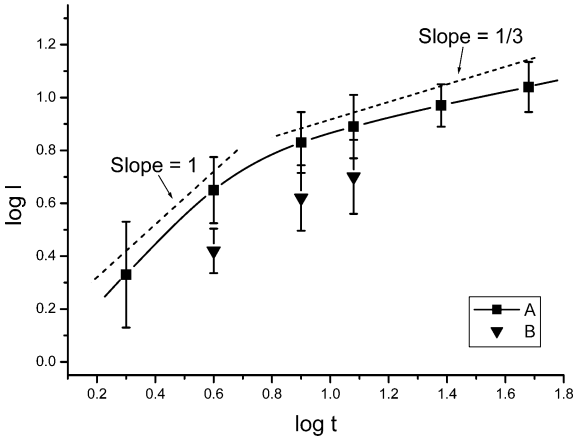

Figure 6. Domain size $l(t)$ plotted vs time t in a log−log plot: (A) average dimension of the droplets obtained through FFT process; (B) number-averaged dimension of the etched cavities calculated from Figure 7b−d.

coarsening process maybe after the possible cocontinuous structure has broken up into droplets of PEOc in the iPP matrix. In this late-stage regime, growth is controlled by a diffusion (of PEOc droplets) and collision coarsening process. The phase-coarsening kinetics should follow the simple growth law:

$$l \sim \left(\frac{k_B T t}{\eta}\right)^{1/3}$$

where η is the viscosity of the fluid. For an off-critical binary fluid, dimensional analysis suggests the mobility μ of a droplet of size l is of order $1/\eta l$, so the diffusion constant is given by the Einstein relation as $D = \mu k_B T \sim k_B T/\eta l$, where k_B is Boltzmann's constant. The time for the droplet to diffuse a distance of order l (and to coalesce with another droplet) is $t \sim l^2/D \sim \eta l^3/k_B T$, which gives $l \sim (k_B T t/\eta)^{1/3}$.[38] Actually, this diffusion collision−coalescence can be observed in Figure 5e,f

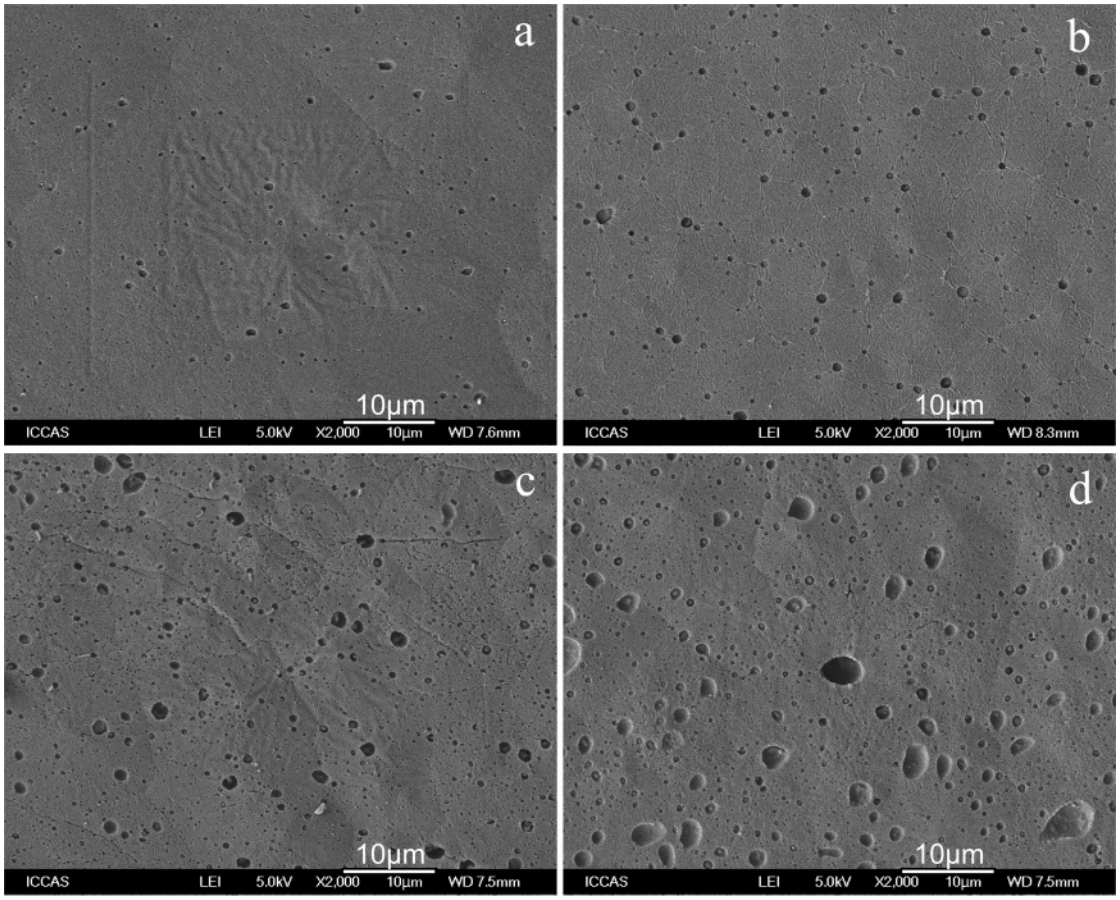

Figure 7. SEM images of the samples undergoing LLPS at 160 °C for (a) 0, (b) 4, (c) 8, and (d) 12 h, followed by rapidly quenching to room temperature and solvent etching.

for many double droplets frozen during the collision and also many halfway coalesced twin particles. All these prove that this iPP/PEOc blend coarsens through a collision−coalescence mechanism instead of a Lifshitz−Slyozov−Wagner evaporation−condensation process which also gives the same $t^{1/3}$ coarsening exponent.

In the present system, phase separation was caused by segregation mainly between the crystallizable iPP and elastomer PEOc. From microscope observations, it could not be decided whether iPP-rich phase or PEOc-rich phase corresponded to the droplets. According to the component proportion, the dispersed phase, namely the droplets, should be the PEOc-rich phase, and the continuous phase should be the iPP-rich phase. To clarify this, a solvent etching technique was used. The phase separation was stopped at $t = 0$, 4, 8, and 12 h by quenching the temperature. Since iPP crystal cannot be dissolved in *n*-heptane at room temperature, whereas elastomer PEOc can be dissolved, the quenched samples were dipped into excessive *n*-heptane at room temperature for about 72 h for selective etching. After the elastomer PEOc component was removed from the sample by washing, spherical shaped cavities appeared on the surface of the sample as shown in Figure 7. These globular cavities should be left by the droplets which had been etched out by solvent. It is clear now that the PEOc-rich phase forms the droplets. In the SEM images, the phase structure is more clearly to be observed, and it shows the same morphological development as in Figure 5: as the LLPS time was increased, the globular cavities grew in size; meanwhile, their size distribution was broadened. The average sizes of cavities estimated from Figure 7b−d are also shown in Figure 6 (symbolized by triangle). They are smaller than the corresponding droplet size obtained by FFT from Figure 5. It may be due to the incomplete dissolution of the elastomer component or due to the number-averaged dimension calculated by hand instead of a weight-averaged dimension obtained through a scattering equivalent FFT process. However, the increasing trend of droplet size is the same.

Figure 8 shows the process of an iPP spherulite swallowing the previously formed PEOc-rich droplets. Figure 8a is the phase contrast micrograph of a growing iPP spherulite at 140 °C after LLPS at 160 °C for 8 h. It can be seen that many PEOc-rich droplets had already been trapped inside the iPP spherulite. By phase contrast microscopy, it can be also seen that in the liquid phase outside the spherulite PEOc-rich droplets dispersed uniformly in the iPP melt matrix. The area in the white circle shows the spot where the iPP spherulite growth front just met a PEOc-rich droplet. In order to show this process more clearly, polarized optical micrographs were used in Figure 8b−d. It can be seen that the spherulite could not push a relatively large droplet away from its initial place when its crystallization front met it. The space occupied by the droplet could not be replaced and filled by iPP lamella. The spherulite just grew around the droplet, like water flows around a stone, and trapped the droplet inside its crystalline domains. The arrow in Figure 8a indicates the position of a PEOc-rich droplet in the liquid matrix when it was meeting the growth front of the spherulite. The arrow in Figure 8d indicates the position of the same PEOc-rich droplet after it had been trapped inside the spherulite. It shows that the droplet stayed still during the crystallization process. These results indicate that after a relatively long LLPS time and the formation of the PEOc-rich droplets in the matrix, as the iPP component isothermally crystallized at 140 °C, these PEOc-

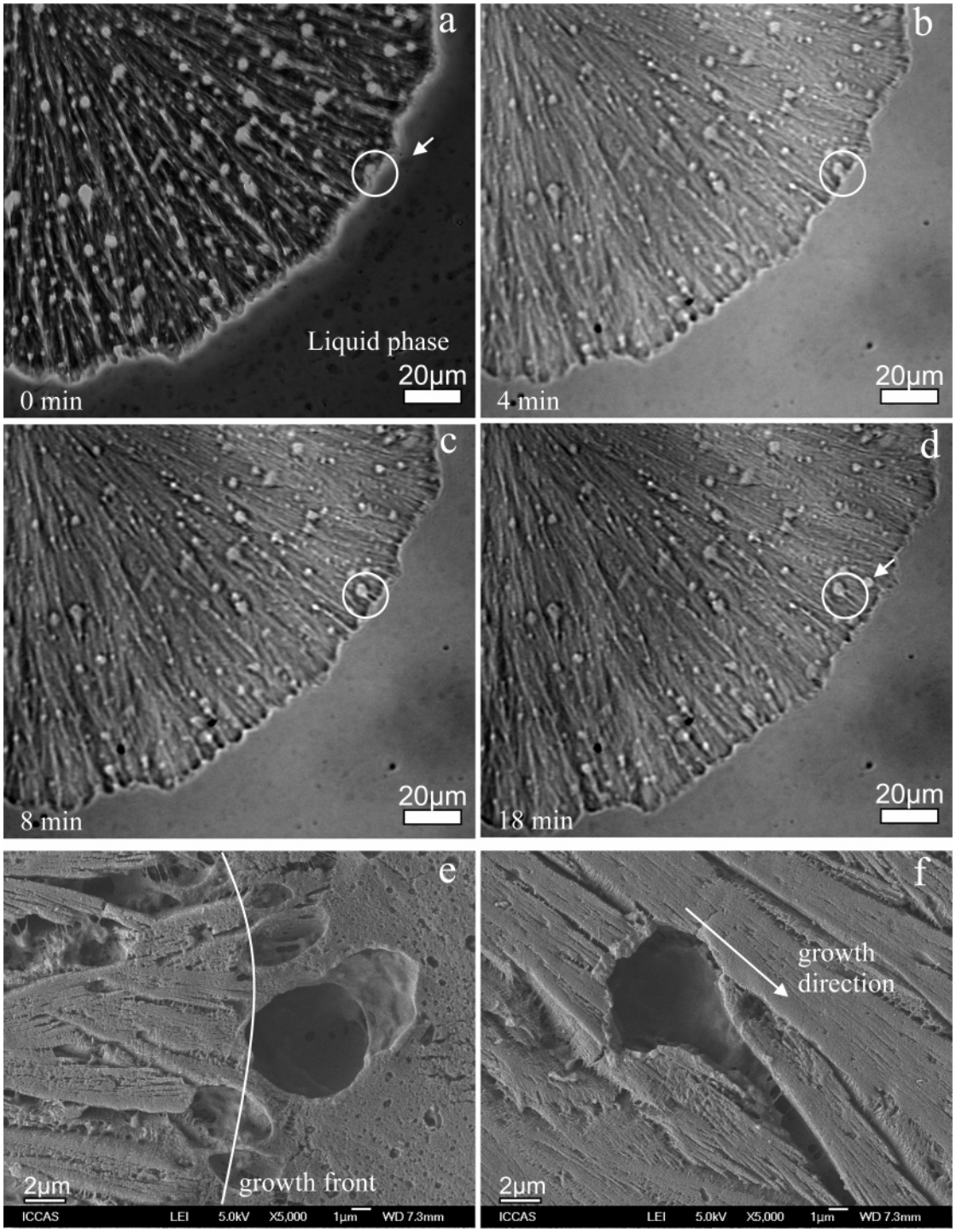

Figure 8. Process of a large iPP spherulite growing round and engulfing the previously formed PEOc-rich droplets.

rich droplets would not change their positions and end up being trapped into the iPP spherulites in situ. The final spatial distribution of the PEOc-rich droplets in the iPP spherulites will be exactly the same as they were in the liquid matrix. Thus, the LLPS structure has a dominant influence on the final crystalline morphology of the sample.

After LLPS at 160 °C for 12 h, the sample, during isothermal crystallization at 140 °C, was quenched to room temperature rapidly and then dipped into *n*-heptane for 72 h. The morphology of the growing iPP spherulites was frozen and maintained. After solvent etching, the elastomer PEOc component dissolved and the iPP crystal remained. So the phase structure is much clearer for observation. Figure 8e is the SEM image near the position where the growth front of an iPP spherulite just met a PEOc-rich droplet. The spherical-shaped cavity was left by the PEOc-rich droplet after solvent etching. It can be seen that the lamella grew in the radial direction of the spherulite. When the lamella met the droplet, the growth stopped. It is because that such droplets are the elastomer-rich domains there are not enough crystallizable materials available for the secondary nucleations in these regions to sustain the crystal growth. Therefore, the lamella that ran directly into the droplets could not grow forward anymore, whereas neighboring lamella grew in a normal way. Figure 8f shows the SEM image of a spherical-shaped cavity inside the iPP spherulite left by a trapped PEOc-rich droplet after solvent etching. No iPP lamella can be seen in the cavity, indicating that iPP lamella could not grow through such elastomer-rich domains. It can be seen that the lamella passing

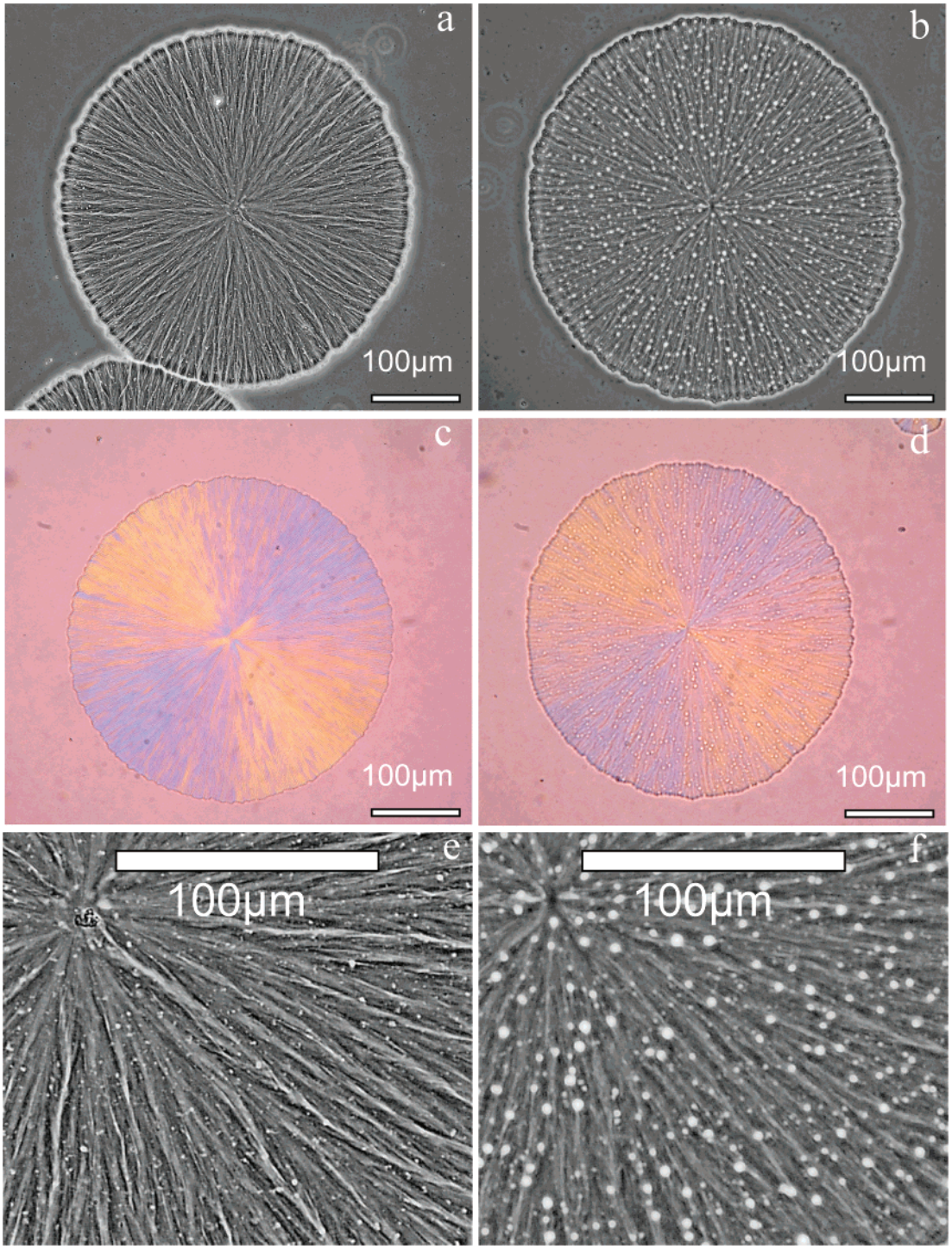

Figure 9. Optical micrographs of the iPP spherulites isothermally crystallized at 140 °C after undergoing LLPS at 160 °C for 0 h (a, c, e) and 12 h (b, d, f); (a) and (b) are the phase contrast micrographs; (c) and (d) are the polarized micrographs taken by means of a primary red filter (λ-plate); (e) and (f) show higher magnification of (a) and (b), respectively.

by the side of the cavity (droplet) filled the space at the back of the cavity (droplet) in the growth direction after certain distance. Thus, in the optical photographs it showed that the iPP spherulites grew around the PEOc-rich droplets which they met. Also, some deformation of the droplets caused by the crystalline growth are sometimes observed.

Figures 5 and 7 have shown that as the annealing time at 160 °C was increased, the coarsening process in the LLPS proceeded, and the uniformly dispersed PEOc-rich droplets grew bigger and bigger. So it can be predicted that if the sample undergoes longer LLPS time, more PEOc component will be coarsened into bigger PEOc-rich droplets which will be trapped in the iPP spherulites rather than being pushed out into the interphase of the spherulites when the sample is isothermally crystallized at 140 °C. Figure 9 displays the phase contrast optical micrographs and the polarized optical micrographs of the iPP spherulites isothermally crystallized at 140 °C after LLPS at 160 °C for 0 and 12 h, respectively. It can be seen very clearly that the average size of the PEOc-rich droplets that dispersed in the iPP spherulites increased with the LLPS time, which shows the same trend as in Figures 5 and 7. In Figure 9a, the average diameter of the droplets was less than 1 μm. In Figure 9b, the biggest droplets increased to about 10 μm, much larger than those in Figure 9a. As the size of the elastomer-rich

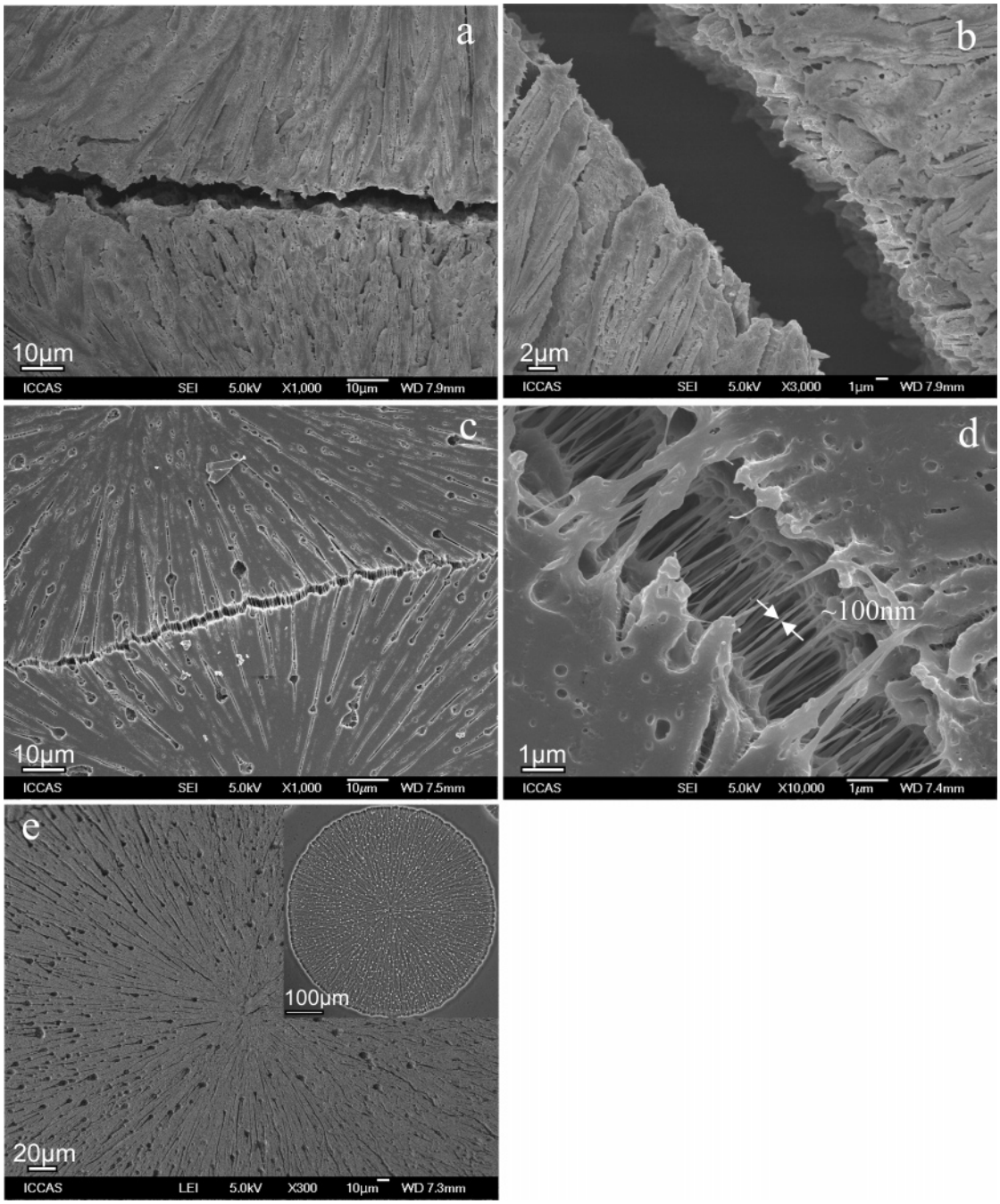

Figure 10. SEM images showing the morphological differences of the samples isothermally crystallized at 140 °C after undergoing LLPS at 160 °C for 0 h (a, b) and 12 h (c−e). The samples were etched by solvent.

droplets increased, the size distribution of these droplets also broadened correspondingly (which were more clearly showed in Figure 9e,f). However, the spatial dispersion of these droplets in the iPP spherulites was fairly uniform all the time. This result is very important because it means that we could control the sizes of the elastomer-rich droplets which remain uniformly dispersed in the crystalline phase. By simply changing the LLPS time, we could continuously adjust the sizes of the elastomer droplets (for example, between 1 and 10 μm) through a $t^{1/3}$ scaling and obtain a series of products with different properties. We could obtain the designed iPP products with specific-sized elastomer droplets that uniformly dispersed in it, according to our need. In addition, a systematic series of materials could be provided for the research of toughening effect of the elastomer droplets with different sizes and size distribution.

Figure 9 also shows that, with increasing the LLPS time, more elastomer PEOc component was trapped in the iPP spherulites and less was rejected outside the spherulites. It is consistent with the results shown in Figures 2−4. In order to see the final distribution of the crystal phase and the elastomer phase more clearly, two samples, crystallized at 140 °C to the completion of spherulite growth after LLPS at 160 °C for 0 and 12 h, were dipped into *n*-heptane for 72 h to etch away the elastomer component and then observed by SEM. It can be seen that after solvent etching deep grooves appeared at the interspherulite boundaries, as shown in Figure 10a,c. These grooves were left by the PEOc-rich phase which had been etched out. The grooves between adjacent spherulites were much wider for the sample directly crystallized at 140 °C without LLPS at 160 °C, which implies that more elastomer components were accumulated at

the interspherulite regions. Besides the deep grooves between adjacent spherulites, many globular cavities were observed inside the spherulites after solvent etching. These intraspherulite globular cavities came from the dissolution of the PEOc-rich droplets engulfed inside the iPP spherulites. It can be seen very clearly that as the annealing time was increased from 0 to 12 h for LLPS, the intraspherulitic globular cavities became much bigger, which implies that more elastomer components were left behind in the spherulites as droplets. And the cavities (droplets) dispersed fairly uniformly in the spherulites, as shown in Figure 10e. These are consistent with the results obtained by the optical microscope observations above. However, there are other considerations that we cannot rule out at this time. One is that the rejection of the PEOc from the bulk of the crystallizing phase maybe also depends on the PEOc composition in the iPP-rich phase. It is likely that the iPP-rich phase is better purified after longer phase separation; less amount of noncrystallizable PEOc needs to be rejected. On the other hand, for short or no prior phase separation, the PEOc concentration is high in the iPP-rich phase, resulting in a thicker layer accumulated at the crystal growth front and the spherulite boundary in the end. The other is the relative rate of the crystal growth and diffusion according to the classical theory.

What unexpected is that there were numerous iPP fibers in the grooves between adjacent spherulites in the sample which had undergone LLPS at 160 °C for 12 h before crystallization at 140 °C, as shown in Figure 10c,d. The width of a typical iPP fiber was measured to be about 100 nm, as indicated in Figure 10d. These iPP fibers tightly linked different spherulites together. Such fibrous linking would produce great effect on the impact property of the material. On the other hand, there were no such iPP fibers in the grooves if the sample was directly crystallized at 140 °C without annealing at 160 °C, as shown in Figure 10b. It seems that the formation of these interspherulite iPP fibers was also dominated by the LLPS process. It is conjectured at this point that the interspherulite fibers connections formed for the samples with a 12 h LLPS annealing may be caused by the merging and rearrangement of intermittently connected interface between the two neighboring spherulites separated by partially continuous elastomer interphases. The connected parts of the two spherulites may be drawn out into fibril-like structures during the further temperature cooling and shrinking of the spherulites. More detailed information on the formation of the iPP fibers between adjacent spherulites will be discussed in a forthcoming paper.

Conclusions

The results presented in this paper show that the LLPS process has a dominant effect on the final crystalline morphology of the iPP/PEOc in-reactor polymer alloy. As the LLPS time was increased, more and more elastomer component was dispersed uniformly in the iPP spherulites as droplets, instead of being rejected to the outside and concentrated at the boundaries of the spherulites, when the sample was isothermally crystallized. It was found that the PEOc component phase separated and coarsened to droplets of certain size after LLPS. The growing spherulites could not push these droplets away from their initial places during crystallization. The iPP spherulites just grew around the elastomer droplets and trapped them in situ. By simply changing the LLPS time, we could continuously adjust the size of the elastomer droplets (for example, between 1 and 10 μm) with uniform spatial dispersion in the iPP spherulites and obtain a series of products with different properties. Meanwhile, a special structural feature which has different iPP spherulites linked together by numerous iPP fibers separated by interconnected elastomer domains was observed by SEM for the first time. The formation of these interspherulite iPP fibers was also dominated by the LLPS process.

The uniformly dispersed intraspherulite elastomer droplets and the numerous interspherulite iPP fibers could potentially make great improvement of the mechanical properties of the iPP/PEOc in-reactor polymer alloy. This in-reactor blending/alloying process provides a new, flexible, and maybe better way to control the structure, dispersion, and finally the properties of elastomer-toughened iPP alloys.

References and Notes

(1) Fernando, P. L.; Williams, J. G. *Polym. Eng. Sci.* **1981**, *21*, 1003.
(2) Narisawa, I. *Polym. Eng. Sci.* **1987**, *27*, 41.
(3) Bramuzzo, M. *Polym. Eng. Sci.* **1989**, *29*, 1077.
(4) Prentice, P.; Williaams, J. G. *Plastics Rubber Proc. Appl.* **1982**, *2*, 27.
(5) Yang, D. C.; Zhang, B. L.; Yang, Y. K.; Fang, Z.; Sun, G. F. *Polym. Eng. Sci.* **1984**, *24*, 612.
(6) Bartczak, Z.; Galeski, A.; Martuscelli, E.; Janik, H. *Polymer* **1985**, *26*, 1843.
(7) Jiang, B. Z.; Uhlmann, D. R.; Vander Sande, J. B. *J. Appl. Polym. Sci.* **1985**, *30*, 2485.
(8) Van Gisbergen, J. G. M.; Meijer, H. E. H.; Lemstra, P. J. *Polymer* **1989**, *30*, 2153.
(9) Van Gisbergen, J. G. M.; Hoeben, W. F. L. M.; Meijer, H. E. H. *Polymer* **1991**, *31*, 1539.
(10) Sun, Z. H.; Yu, F. S.; Qi, Y. C. *Polym. Acad.* **1991**, *2*, 143.
(11) Choudhary, V.; Varma, H. S.; Varma, I. K. *Polymer* **1991**, *32*, 2534.
(12) Choudhary, V.; Varma, H. S.; Varma, I. K. *Polymer* **1991**, *32*, 2541.
(13) D'Orazio, L.; Mancarella, C.; Martuscelli, E. P. *Polymer* **1991**, *32*, 1186.
(14) D'Orazio, L.; Mancarella, C.; Martuscelli, E.; Sticotti, G.; Massari, P. *Polymer* **1993**, *34*, 3671.
(15) Chiang, W. Y.; Yang, W. D.; Pukanszky, Bela. *Polym. Eng. Sci.* **1992**, *32*, 641.
(16) Galli, P.; Haylock, J. C. *Makromol. Chem., Macromol. Symp.* **1992**, *63*, 19.
(17) Galli, P.; Vecellio, G. *Prog. Polym. Sci.* **2001**, *26*, 1287.
(18) Cecchin, G. *Macromol. Symp.* **1994**, *78*, 213.
(19) Galli, P.; Collina, G.; Sgarzi, P.; Baruzzi, G.; Marchetti, E. *J. Appl. Polym. Sci.* **1997**, *66*, 1831.
(20) Cai, H.; Luo, X.; Ma, D.; Wang, J.; Tan, H. *J. Appl. Polym. Sci.* **1999**, *71*, 93.
(21) Cai, H.; Luo, X.; Ma, D.; Wang, J.; Tan, H. *J. Appl. Polym. Sci.* **1999**, *71*, 103.
(22) Wang, L. X.; Huang, B. T. *J. Polym. Sci., Part B: Polym. Phys.* **1990**, *28*, 937.
(23) China Pat CN1982341.
(24) Feng, Y.; Hay, J. N. *Polymer* **1998**, *39*, 6723.
(25) Fan, Z.; Zhang, Y.; Xu, J.; Wang, H.; Feng, L. *Polymer* **2001**, *42*, 5559.
(26) Xu, J.; Fu, Z.; Fan, Z.; Feng, L. *Eur. Polym. J.* **2002**, *38*, 1739.
(27) Zhang, Y.; Fan, Z.; Feng, L. *J. Appl. Polym. Sci.* **2002**, *84*, 445.
(28) Fu, Z.; Fan, Z.; Zhang, Y.; Feng, L. *Eur. Polym. J.* **2003**, *39*, 795.
(29) Manson, J. A.; Sperling, L. H. *Polymer Blends and Composites*; Plenum Press: New York, 1976.
(30) Bucknall, C. B. *Toughened Plastics*; Applied Science Publishers: London, UK, 1977.
(31) Liu, N.; Baker, W. *Polymer* **1994**, *35*, 988.
(32) KuKaleva, N.; Jollands, M.; Cser, F.; Kosior, E. *J. Appl. Polym. Sci.* **2000**, *76*, 1011.
(33) Prentice, P. *Polymer* **1982**, *23*, 1189.
(34) Yeh, P. L.; Birley, A. W.; Hemsley, D. A. *Polymer* **1985**, *26*, 1155.
(35) Besomles, M.; Menguel, J.-F.; Delmas, G. *J. Polym. Sci., Part B: Polym. Phys.* **1988**, *26*, 1881.
(36) Karger-Kocsis, J.; Kiss, L.; Kuleznev, V. N. *Polym. Commun.* **1984**, *25*, 122.
(37) Keith, H. D.; Padden, F. J. *J. Appl. Phys.* **1964**, *35*, 1270.
(38) Furukawa, H. In *Structure and Properties of Multiphase Polymeric Materials*; Araki, T., Tran-Cong, Q., Shibayama, M., Eds.; Marcel Dekker: New York, 1998; Chapter 2, p 35.

MA7021869